

Landsat Image Analysis of Tree Mortality in the Southern Sierra Nevada Region of California during the 2013-2015 Drought

Christopher S Potter*

NASA Ames Research Center, Mail Stop 232-21, Moffett Field, CA, USA

Abstract

The United States Forest Service (USFS) observed marked increases in tree mortality in the southern Sierra Nevada foothills and mountains of California using aerial monitoring surveys in April 2015. Aircraft flew over 4 million acres of forested land and found that about 20 percent of forest stands had detectable mortality, totaling 10.45 million dead trees. In this study, Landsat satellite imagery was analyzed at over 90% of these high tree mortality sites in the southern Sierra to understand how the three consecutive years (2013-2015) of extreme drought conditions compared to changes in forest stand growth rates dating to the mid-1980s across this region. Results showed that changes in Landsat drought-sensitive indices from the years 2011 to 2015 closely matched patterns of tree mortality across USFS April 2015 aerial survey locations in the southern Sierra Nevada. The historically low snow year of 2015 could have essentially reset the average forest canopy density for many forests in the region to late 1980s levels, due to drought-related mortality, combined with numerous large stand-replacing wildfires. The corresponding patterns and trends in Landsat drought-sensitive indices with observed tree mortality rates can better inform region-wide assessments of forest growth trends and enable long-term drought impact monitoring.

Keywords: Landsat; Forest; Normalized difference vegetation index (NDVI); NDMI; Drought; Disturbance; Sierra Nevada; California

Introduction

Drought impacts on the vigor and long-term survival of forests across the state of California have become a pressing concern among scientists, water supply agencies, and land managers. Alarming projections of future tree mortality across the western United States have been linked to potential transforms of ecosystem structure, tree species composition, loss of biodiversity, and increased wildfire risks [1].

In April 2015, the United States Forest Service (USFS) flew more than 4.1 million forested acres in the southern Sierra Nevada region of California, with aerial surveys covering the low elevation western portions of the Stanislaus, Sierra and Sequoia National Forests (NF) and Yosemite and Sequoia-Kings Canyon National Parks [2]. The locations of dead and dying trees were recorded visually by a surveyor, using a digital sketch-mapping system on a fixed-wing aircraft flying approximately 330 meters above ground level. The surveyor recorded the number and species of affected trees and type of damage (mortality, defoliation, etc.) at each mapped location.

These surveys mapped the locations of 10.45 million recently dead trees in the region. In the Sierra foothills, tree mortality was widespread, especially in ponderosa pine, gray pine, and potentially in blue oak and live oak. On the Stanislaus NF, mortality was scattered in northern areas, but roughly doubled since July 2014 in extensive ponderosa and other pine forests in the southern low-elevations areas. At higher elevations, conifer mortality was scattered. On the Sierra and Sequoia NFs, tree mortality, mostly from western pine beetle, was common almost everywhere at lower elevations [2].

Satellite remote sensing has been shown to be an effective method to measure large-scale patterns of vegetation biomass and tree growth rates in remote mountain areas [3-11]. van Wageningen and Root [12] reported that the satellite normalized difference vegetation index (NDVI) can provide information necessary to distinguish vegetation types when analyzed over a summer growing season in the Sierra Nevada. Similar studies have found that NDVI is sensitive to early

(herbaceous) post-fire recovery and subsequent woody (tree and shrub) regrowth trajectories [13,14]. Schiffman [15] reported a strong correlation ($R^2 = 0.7$) between July Landsat NDVI and leaf area index (LAI) measured in 175 forest stands of Yosemite National Park.

LAI is an important indicator of forest stand condition, chiefly because of its close relation to canopy photosynthesis and transpiration rates [16]. Comparisons with field measurements have shown that remotely sensed NDVI from surface reflectance was significantly correlated with both LAI and with annual growth increments in coniferous forests and woodlands stands, including those in the western United States [17-20], and did not saturate until LAI levels were far greater than those commonly reported for forest stands of the subalpine Sierra Nevada.

In a regional study of annual moisture availability and forest greenness variations over 25 years, Trujillo et al. found a strong positive relationship between Sierra Nevada forest NDVI and maximum annual snow accumulation. The correlation between annual peak (July - August) satellite NDVI (at 8-km spatial resolution) and peak snow water equivalents (SWE) for evergreen needle leaf forests in the northern and central Sierra Nevada was between R^2 of 0.7 and 0.8 over the period of 1982 to 2006. This study implied that the level to which snow accumulation can explain inter-annual variations in Sierra forest green cover is highest in the elevation zone between 2000 and 2600 m.

For additional mapping of drought impacts on forest stands, the Landsat normalized difference moisture index [21] has been validated

*Corresponding author: Christopher S Potter, NASA Ames Research Center, Mail Stop 232-21, Moffett Field, CA, USA, Tel no: 650-604-6164; E-mail: chris.potter@nasa.gov

Received March 13, 2016; Accepted March 28, 2016; Published March 31, 2016

Citation: Potter CS (2016) Landsat Image Analysis of Tree Mortality in the Southern Sierra Nevada Region of California during the 2013-2015 Drought. J Earth Sci Clim Change. 7: 342. doi:10.4172/2157-7617.1000342

Copyright: © 2016 Potter CS. This is an open-access article distributed under the terms of the Creative Commons Attribution License, which permits unrestricted use, distribution, and reproduction in any medium, provided the original author and source are credited.

in the field repeatedly as an index of vegetation canopy moisture status [22-24], including impacts of insect outbreaks on western conifer forests [25]. Potter [26] and Van Gunst et al. [27] showed that the NDMI can be used to monitor and map year-to-year variations in drought stress across California forest and woodland ecosystems.

The objective of the present study was to analyze 30 consecutive years of Landsat NDVI and NDMI values (at 30-m spatial resolution) at USFS aerial survey locations in the southern Sierra forest that showed the high levels of tree mortality in April 2015, to gain a better understanding of what yearly satellite observations can track in terms of changes in stand structure and forest canopy variations. The calendar year 2013 was the driest on record in California, with a total of just 30% of average statewide precipitation [28]. A record low snowpack level in 2015 in the Sierra Nevada Mountains was unprecedented in comparison to the past 500 years [29], with SWE levels measured across the Sierra region of only 5% of the historical average. Landsat's unique three-decade record of vegetation cover change provides a rich archive, within which to put the 2013-2015 drought into historical perspective, particularly with respect to the impacts of observed tree mortality on stand canopy density, drought stress, and LAI.

Study area

The Sierra Nevada region covers over 63,000 km² along a north-south axis of California. Rundel et al. [30] defined elevation zones in the Sierra-Nevada roughly as: montane (1500 - 2500 m), subalpine (2500 - 3000 m), and alpine (above 3000 m). Before human settlements in the mid-1800s, conifer forests throughout the region experienced wildfires mainly of low and moderate severity. Montane zone pine and mixed-conifer forests historically experienced mean fire return intervals of 11 to 16 years [31]. In higher elevation subalpine forests of the Sierra Nevada, the typical pre-settlement fire return intervals were between 35-100 years [32].

Among the most common tree species in the montane zone are ponderosa pine (*Pinus ponderosa*), Douglas fir (*Pseudotsuga menziesii*), white fir (*Abies concolor*), incense cedar (*Calocedrus decurrens*), black oak (*Quercus kelloggii*), and interior live oak (*Quercus wislizeni*). The most common tree species in the subalpine zone are whitebark pine (*P. albicaulis*), lodgepole pine (*P. contorta subs. murrayana*), mountain hemlock (*Tsuga mertensiana*), western white pine (*P. monticola*), red fir (*Abies magnifica*), Sierra juniper (*Juniperus occidentalis var. australis*), Jeffrey pine (*P. jeffreyi*), and white fir [32].

Average annual precipitation in the central Sierra ranges from 80 cm at lower elevations to more than 170 cm at higher elevations, with most precipitation falling during the winter as snow [33]. Peak annual SWE levels range from 50 cm to 160 cm, depending on elevation and topography [34].

Methods

Satellite Image Processing

Near cloud-free imagery from the Landsat sensor was selected from the U. S. Geological Survey Earth Explorer data portal (<http://earthexplorer.usgs.gov/>) for every year from 1985 to 2015, with the exception of 2012 that was missed during the transition from Landsat 5 to Landsat 8 satellites. Image data from Landsat path/rows 41/35 and 42/34 were acquired between July 15 and August 30 each year, around the peak of the Sierra summer growing season [12,34]. All images used in this study were geometrically registered (UTM Zone 10) using terrain correction algorithms (Level 1T) applied by the U. S. Geological Survey EROS Data Center [35].

For the Landsat 4-5 Thematic Mapper (TM) images acquired 30-m resolution surface reflectance data were generated from the Landsat Ecosystem Disturbance Adaptive Processing System [36]. Moderate Resolution Imaging Spectroradiometer (MODIS) atmospheric correction routines were applied to Level-1 TM data products. Water vapor, ozone, geopotential height, aerosol optical thickness, and digital elevation are input with Landsat data to the Second Simulation of a Satellite Signal in the Solar Spectrum (6S) radiative transfer models to generate top of atmosphere (TOA) reflectance, surface reflectance, brightness temperature, and masks for clouds, cloud shadows, adjacent clouds, land, snow, ice, and water. After 2012, Landsat 8 surface reflectance products were generated from the L8SR algorithm [36], a method that uses the scene center for the sun angle calculation and then hard-codes the view zenith angle to 0. The solar zenith and view zenith angles are used for calculations as part of the atmospheric correction.

NDVI calculation

Cloud- and snow-filtered NDVI images were generated as the differential reflectance between the red and near-infrared (NIR) portions of the spectrum by the equation:

$$NDVI = (NIR - Red) / (NIR + Red)$$

and scaled from 0 to 10000, where NIR is the reflectance of μm wavelengths from 0.76 to 0.9 and Red is μm . Low values of NDVI (near 0) indicate barren land cover whereas high values of NDVI (near 8000) indicate dense canopy vegetation cover. Van Wagendonk and Root [12] reported that July-August NDVI values greater than 5000 corresponded to high densities of conifer forest and shrubland (chaparral) cover of Yosemite National Park in the central Sierra Nevada. Schiffman [15] found that summer NDVI values greater than 5000 corresponded to an LAI above 1 and NDVI values greater than 7000 corresponded to an LAI above 3 in forests of Yosemite National Park.

NDMI calculation

The severity of drought stress across the study region was determined using the Landsat NDMI [21], computed by the equation:

$$NDMI = (NIR - SWIR) / (NIR + SWIR)$$

Where, SWIR is the short wave infrared (SWIR; 1.55 - 1.75 μm) band. NDMI (scaled 0 to 10000) is comparable to the Landsat normalized burn ratio (NBR) used for wildfire severity mapping [37]. The reduction of reflectance of the SWIR as compared to the NIR is due to the absorption of water in leaf tissues [38]. High NDMI values represent relatively high vegetation canopy moisture and lower drought stress, while near-zero values would represent relatively low vegetation canopy moisture content and higher drought stress [26].

Other data sets used

Elevation, slope, and aspect at 1 arc-second resolution were determined from the United States Geological Survey (USGS) National Elevation Dataset (NED). Wildfire boundaries and years since fire (YSF) were compiled from the California Department of Forestry, Fire and Resource Assessment Program (FRAP; data available at <http://frap.cdf.ca.gov/>), with additions from the National Park Service.

Data analysis

Yearly NDVI values from 1985 to 2015 at approximately 2020 USFS aerial survey locations (depending on seasonal cloud cover) within Landsat path/row 41/35 and 42/34 areas (Figure 1) were averaged

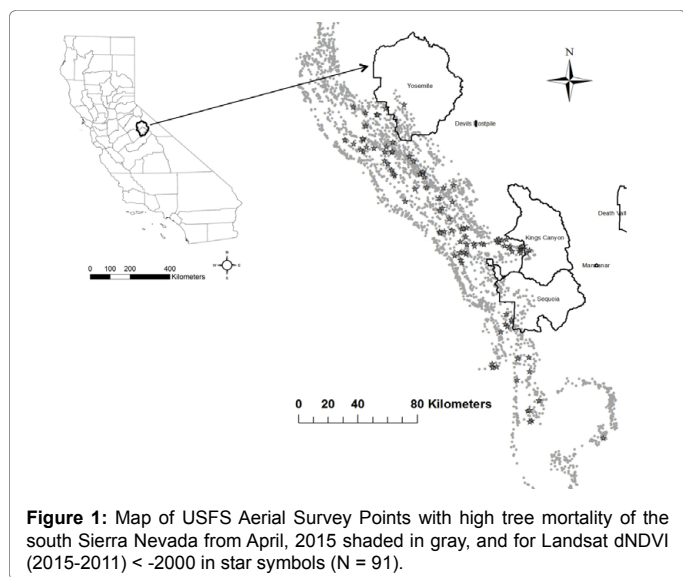


Figure 1: Map of USFS Aerial Survey Points with high tree mortality of the south Sierra Nevada from April, 2015 shaded in gray, and for Landsat dNDVI (2015-2011) < -2000 in star symbols (N = 91).

and subjected to time series non-linear (second-order polynomial) regression analysis. A significant difference from zero, or between two (yearly) sample means of NDVI or NDMI at 95% confidence ($p < 0.05$), was based on the finding of a separation of the mean(s) at greater than (plus or minus) 2 standard errors [39]. Correlations between NDVI (or NDMI) change values at these aerial survey locations with observed tree mortality were also computed versus latitude, elevation, slope, aspect, and YSF.

Results

NDVI and NDMI time series analysis

For yearly NDVI averaged across all USFS 2015 aerial survey locations with high observed tree mortality, variations over the time period of 1985 to 2015 were dominated by three major periods of extreme low SWE recorded for the Sierra Nevada region [29,34,40], specifically 1988-1990, 2000-2001, and 2013-2015 (Figure 2). Yearly NDVI declined by 500-700 units (about 10%) during each of these three drought periods. Between each of these drought periods, average NDVI for all April 2015 aerial survey locations recovered rapidly to average pre-drought levels and then increased to exceed those levels by at least 500 NDVI units, or about 10% of 1985 average NDVI levels.

With focus on the most recent drought period, average NDVI in August 2015 for all USFS aerial survey locations with observed tree mortality in April 2015 was significantly lower than average NDVI in 2011 (pre-drought) or in 2013 ($p < 0.05$). Despite this significant decline in average NDVI from 2011 to 2015, the average NDVI in 2015 was higher than average NDVI in 1990 or in 2002 -- the years at the ends of the previous two periods of extreme drought in the Sierra Nevada.

Nonetheless, the Landsat record showed a major decline of 18% in average NDMI between 2011 and 2015 (Figure 2) for the USDA aerial survey locations, which was statistically significant ($p < 0.05$) and greater than the change in average NDVI for the same set of April 2015 aerial survey locations. The apparent drought stress detected by the steep downward change in NDMI began in 2013 and proceeded at equal downward intervals in both 2014 and 2015.

Average NDMI in 2015 for all USFS aerial survey locations with observed tree mortality in April 2015 was significantly lower ($p < 0.05$)

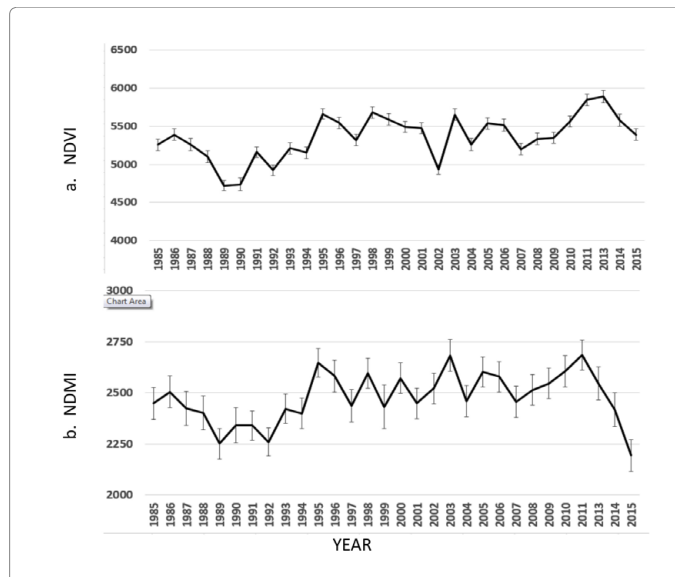


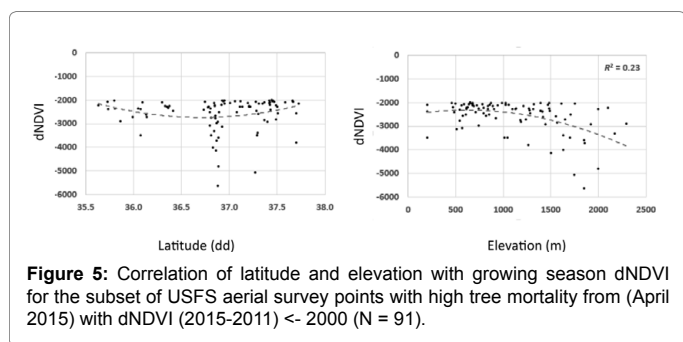
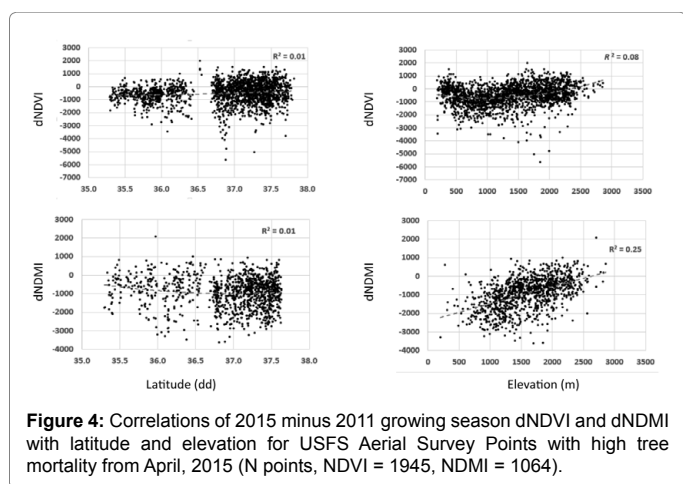
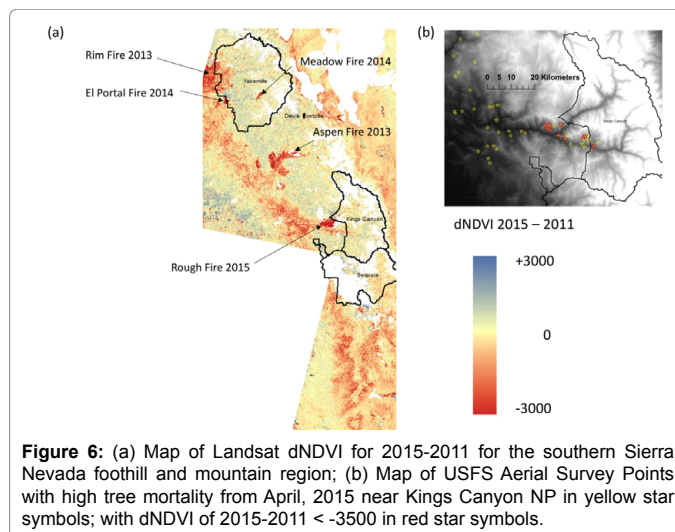
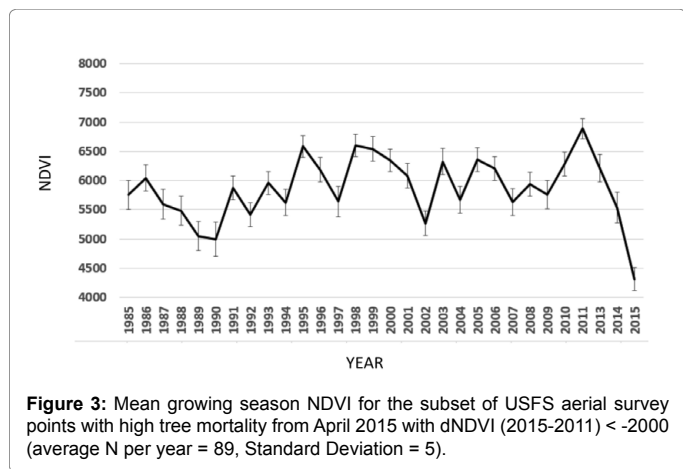
Figure 2: Mean growing season (a) NDVI and (b) NDMI for USFS Aerial Survey Points with high tree mortality from April, 2015 (average N per year, NDVI = 2021 Standard deviation = 99; NDMI = 1440 Standard deviation = 177).

than average NDMI in any other year of the 30-yr time series, with the exception of the years 1989 – 1992. Similarly, the negative change in NDVI between 2011 and 2015 (Figure 3) for these aerial survey locations that exceeded a threshold of more than 20% (< -2000 NDVI units; N = 89) together showed a similar overall to the 30-yr time series of NDMI.

Average NDVI variations with topography

Slope, aspect, and YSF at the USDA aerial survey locations with high observed tree mortality in April 2015 were each correlated separately in non-linear regression analyses with the Landsat image differences (dNDVI or dNDMI) between 2015 and 2011. None of these three geographic variables explained a significant portion of the variation among the sampled 2015-2011 dNDVI or dNDMI values. All these resulting R^2 correlation values for dNDVI and dNDMI were lower than 0.05 in the regression analysis results. It is worth noting however that the majority of aerial survey locations with the most extreme negative 2015-2011 dNDVI values (in excess of -2000 units) were detected at slopes between 15% and 30%.

The correlations with latitude of sampled 2015-2011 dNDVI or dNDMI values at the USDA aerial survey locations with observed tree mortality in April 2015 were not significant, although the most extreme negative 2015-2011 dNDVI and dNDMI values were located mainly between 36° and 37° N latitude (Figure 4). The correlation with elevation of sampled 2015-2011 dNDMI values at the USDA aerial survey locations was significant ($p < 0.05$) and showed that most of the extreme negative 2015-2011 dNDMI values in excess of -2000 units were detected at elevations below 2000 m. The correlation with elevation for the most extreme negative 2015-2011 dNDVI values was also significant ($p < 0.05$; Figure 5), but in contrast to dNDMI, showed a decreasing pattern of dNDVI with increasing elevation, starting at 1200 m to approximately 2300 m elevation. This may be due, in part, to the predominately lower elevation (< 2100) survey coverage of the April 2015 USDA flights; whereas surveys later in the summer detected extensive tree mortality at higher elevations in the southern Sierra.



Locations of greatest negative NDVI change

A regional scale view of 2015-2011 dNDVI values mapped from Landsat imagery over the study area (Figure 6) showed extensive areas of negative dNDVI (in excess of -2000 units) on the southwestern margins of Yosemite NP, Kings Canyon NP, and Sequoia NP, and Sierra and Sequoia NF boundaries (Figure 6). For comparison of these apparent drought impacts on tree die-back, the areas within five large wildfires that occurred across the region in the period of 2013 to 2015 showed 2015-2011 negative dNDVI values in excess of -3000 units. The majority of USDA aerial survey locations with observed tree mortality in April 2015 at which negative 2015-2011 dNDVI values were detected in excess of -3000 units fell within the July 2015 Rough Fire perimeter,

which started on the western boundary of Kings Canyon NP and burned into Cedar Grove during September 2015.

Discussion

Results from this study indicate that changes in Landsat drought-sensitive indices from 2011 to 2015 matched patterns of tree mortality across USFS April 2015 aerial survey locations in the southern Sierra Nevada. Both NDVI and NDMI had been increasing steadily since early 1990s across these aerial survey locations, which was indicative of infilling by relatively young forest stands with high stem densities [41,42]. Drought and the historically low snow year of 2015 may have essentially reset the average forest canopy density (per LAI and water use) for many forests in the region to late 1980s levels, due to drought related mortality and stand removal by large wildfires.

In support of these conclusions, the evidence strongly linking satellite NDVI and NDMI to forest growth and decline patterns comes from a series of previous ground validation studies in the Sierra Nevada. For instance, forest stand NDVI values greater than 5000 have been correlated with dense foliar cover in conifer forest stands in the Sierra (van Wagtenonk and Root, 2003). Schiffman (2008) also reported a close correlation between NDVI and leaf area index (LAI) measured across Sierra forest stands. These and other ground-truth studies [17,18] have established NDVI as a reliable remotely sensed surrogate for variations in stand LAI and canopy biomass in this montane region.

Several field measurement data sets of conifer forest growth and stand structure in the western U. S. have repeatedly demonstrated a strong linear relationship between LAI and stem basal area growth. For example, Kashian et al. [43] showed a significant relationship ($R^2 = 0.6$, $p < 0.01$) between LAI and basal area increment (BAI) for 48 lodgepole pine stands aged 45-350 years in Yellowstone National Park, Wyoming. Stem density at the stand level was weakly correlated with both LAI and BAI ($R^2 = 0.22$) overall and was uncorrelated with either LAI or BAI at stand age classes less than 200 years old. Previous measurements by Knight et al. [44] at eight stands of lodgepole pine in the Medicine Bow Mountains of southeastern Wyoming showed the same basic patterns between LAI, basal area, and stem density. Peterson et al. [45] reported a significant correlation ($R^2 = 0.9$, $p < 0.01$) between LAI and BA across six lodgepole and whitebark pine stands in the Eastern Brook Lakes watershed of the Inyo National Forest in the Sierra Nevada. Stem density at the stand level here was uncorrelated here with either LAI or BA

($R^2 = 0.1$). Based on this review of numerous field plot measurements, LAI and (hence NDVI) should be a reliable predictor of stem growth in Sierra Nevada forest stands.

Ceccato et al. [46] developed and tested an index similar to the NDMI using data from the SPOT satellite sensor. They concluded that the SWIR channel was critical to estimating leaf water content and that the NIR channel was needed to account for variation of leaf internal structure and dry matter content variations. Likewise, Van Gunst et al. [27] used multi-year Landsat NDMI data to examine variations in mortality among forest types and climate periods from 1985 to 2010 in the mixed conifer forest of the Lake Tahoe Basin. Results showed that low Landsat NDMI values (< 2000) were significantly related to low forest canopy vigor and high annual tree mortality rates of $> 20\%$. This study also found that positive density-dependent mortality was associated with lower elevation (below 2100 m) forests and drier climate periods. In mid- to upper-elevation (above 2100 m) forests, increased density was more often associated with decreased probability of mortality, especially during wetter periods. Tree mortality was highest during the drought period of 1988 to 1994, but not in a subsequent drought periods (prior to 2011) of similar severity. Results also suggested increased risk of tree mortality on north-facing slopes across all forests and all climate periods.

Several previous field studies had shed light on the mechanisms of forest decline the Sierra Nevada range. For instance, Smith et al. [47] surveyed trees in the southern Sierra National Forest and reported that pathogen- and insect-associated mortality was significantly greater in areas of high stand density but was not higher for shade-tolerant species. Tree mortality was higher than expected for large-diameter trees, suggesting an acceleration of old- tree mortality under current fire suppression conditions. The overall conclusion of this study was that the increase in stem density due to fire suppression and/or climate change has overwhelmed the corrective nature of mortality by native pathogens and insects in forest of the southern Sierra Nevada range, at least up until the 2013-2015 droughts. Related to this, Dolanc et al. [41] speculated that the decrease in density of large trees in Sierra Nevada subalpine zone over the past 75 years has been consistent with observed changes in climate. Higher temperatures may have shortened the time to drought induced mortality of trees and can increase the susceptibility of conifers to insect attack [33,48]. Guarin and Taylor [49] investigated the influence of drought and topography on patterns of tree mortality in old-growth mixed conifer forests in Yosemite NP. Correlations between tree mortality and drought were evident only for multi-year periods of 2 to 5 years and the frequency of tree death dates was negatively correlated with April snowpack depth recorded since the mid-1970s. The density of dead trees was found to be slightly higher on north- than south-facing slopes, possibly due to competition between white fir and incense cedar seedlings and saplings.

As a comparison to these latest drought study results from the southern Sierra Nevada region, Potter [26] used both Landsat dNDVI and dNDMI to assess the impacts of the 2013-2014 drought on forested ecosystems of the California Central Coast. In contrast to the extensive drought stress detected in the southern Sierra Nevada region (Figure 6), only a small fraction (less than 5%) of all forest cover area in the Central Coast region showed relatively high drought stress. The Central Coast is not snow-dependent in terms of the annual water supply for woody vegetation communities (as is the Sierra Nevada), which, together with a relatively short return interval promoting rapid regrowth between stand replacing wildfires on the coast, may explain the observed lack of a severe drought impact since 2010-11 on forests in this ecosystem.

From a general remote sensing perspective, imaging by hyperspectral sensors (using a relatively narrow band resolution of several nm) can play a role in drought impact monitoring [50], provided that aircraft flights are conducted in a timely, economical, and sustained manner. Findings from tropical forest experiments with hyperspectral imaging have showed that nearly 20% of canopy LAI can observe to be lost from the wet to dry season during enhanced drought conditions [51,52]. Leaf water potential was also highly sensitive to drought, decreasing by almost 30% compared to the control forest. The net effect on remotely sensed hyperspectral data was a measurable lowering of reflectance across the entire NIR spectral range in drought-affected areas, compared with that of unaffected control plots. Similarly, in a hyperspectral sensing study of California oak forest response to moisture stress, Pu et al. [53] reported the same kind of broad, uniform lowering of signal across the entire NIR reflectance spectra. In theory, hyperspectral imaging is better suited to detecting relatively narrow band responses (of several nm) to changing environmental factors. Both Landsat NDVI and NDMI adequately account for the spectrally uniform, broad-band NIR response to drought stress (as commonly seen in hyperspectral imagery), while meeting all the criteria for being timely, economical, and sustained observations spanning over 30 years across all forest ecosystems. The main compromise with Landsat satellite versus airborne imaging is in the spatial granularity of the imagery, from a few meters to 30 m ground resolution.

Conclusions

According to Landsat image mapping, the regional patterns of forest disturbance and potential canopy dieback over the period 2011 to 2015 in the southern Sierra Nevada have resulted from a combination of historically large wildfires and historically low annual snow accumulation amounts. Both Landsat dNDVI and dNDMI time series were found to closely match tree mortality observations from USFS April 2015 aerial survey locations, and verified previously published findings, which indicated that low Landsat NDMI values (a change to below 2000 NDMI units) were significantly related to low forest canopy vigor and high annual tree mortality rates of $> 20\%$. Analysis of Landsat image data in subsequent years around these same southern Sierra Nevada aerial survey locations may assist forest managers in the assessment of delayed tree mortality post-2015, and in tracking subsequent regrowth rates of drought-affected forest stands during more favorable precipitation years.

Acknowledgements

The author thanks Jeffrey Moore (USFS, Davis, California) for valuable comments on the results of this study.

References

1. Anderegg WRL, Flint A, Huang C, Flint L, Berry JA, et al. (2015) Tree mortality predicted from drought-induced vascular damage. *Nature Geosci* 8: 367-371.
2. Moore J, Heath Z, Bulaon B (2015) Aerial Detection Survey - April 15th - 17th 2015, Forest Health Protection Survey, United States Forest Service, pp.6. pp.
3. Collins B, Woodcock CE (1996) An assessment of several linear change detection techniques for mapping forest mortality using multitemporal Landsat TM data. *Remote Sens Environ* 56: 66 -77.
4. Amiro BD, Chen JM, Liu J (2000) Net primary productivity following forest fire for Canadian ecoregions. *Can J For Res* 30: 939-947.
5. Rogan J, Franklin J (2001) Mapping wildfire burn severity in southern California forests and shrub lands using Enhanced Thematic Mapper imagery. *Geocarto Int* 16: 89- 99.
6. Rogan J, Miller J, Stow DA, Franklin J, Levien L, et al. (2003) Land-cover change monitoring with classification trees Using Landsat TM and ancillary data. *Photogramm Eng Remote Sens* 69: 793-804.

7. Fischer L, Rosenberg M, Mahon L, Liu Z, Maurizi B, et al. (2004) Monitoring land cover changes in California, a USFS and GDF cooperative program, Northern Sierra Project Area - Cycle II. State of California, Resources Agency, Department of Forestry and Fire Protection, Sacramento, CA.
8. Epting J, Verbyla DL (2005) Landscape level interactions of pre-fire vegetation, burn severity, and post-fire vegetation over a 16-year period in interior Alaska. *Can For Res* 35: 1367-1377.
9. Cuevas-Gonzalez M, Gerard F, Balzter H, Riano D (2009) Analysing forest recovery after wildfire disturbance in boreal Siberia using remotely sensed vegetation indices. *Global Change Biol* 15: 561-577.
10. Casady GM, Marsh SE, (2010) Broad-scale environmental conditions responsible for post-fire vegetation dynamics. *Remote Sens* 2: 2643-2664.
11. Li S, Potter C (2012) Vegetation regrowth trends in post forest fire ecosystems across North America from 2000 to 2010. *Nat Sci* 4: 755-770.
12. van Wagtenonk JW, Root RR (2003) The use of multi-temporal Landsat Normalized Difference Vegetation Index (NDVI) data for mapping fuel models in Yosemite National Park, USA. *Int J Remote Sens* 24: 1639-1651.
13. Potter C, Li S, Huang S, Crabtree RL (2012) Analysis of sapling density regeneration in Yellowstone National Park with hyperspectral remote sensing data. *Remote Sens Environ* 121: 61-68.
14. Franks S, Masek JG, Turner MG (2013) Monitoring forest regrowth following large scale fire using satellite data - A case study of Yellowstone National Park, USA. *Eur J Remote Sens* 46: 561-569.
15. Schiffman B (2008) Estimation of Leaf Area Index (LAI) through the acquisition of ground truth data in Yosemite National Park, ASPRS 2008. Annual Conference Portland, Oregon.
16. Chen JM, Cihlar J (1996) Retrieving leaf area index of boreal conifer forests using Landsat TM images. *Remote Sens Environ* 55: 153-162.
17. Gong P, Pu R, Miller JR (1995) Coniferous forest leaf area index estimation along the Oregon transect using compact airborne spectrographic imager data. *Photogramm Eng Remote Sens* 61: 1107-1117.
18. Turner DP, Cohen WB, Kennedy RE, Fassnacht KS, Briggs JM (1999) Relationships between leaf area index and Landsat TM spectral vegetation indices across three temperate zone sites. *Remote Sens Environ* 70: 52-68.
19. Wang J, Rich PM, Price K, Kettle W (2004) Relations between NDVI and tree productivity in the central Great Plains. *Int J Remote Sens* 25: 3127-3138.
20. Li S, Potter C, Hiatt C (2012) Monitoring of net primary production in California rangelands using Landsat and MODIS satellite remote sensing. *Nat Res* 3: 56-65.
21. Gao BC (1996) NDWI - A normalized difference water index for remote sensing of vegetation liquid water from space. *Remote Sens Environ* 58: 257-266.
22. Hunt ER, Rock BN (1989) Detection of changes in leaf water content using near and middle-infrared reflectances. *Remote Sens Environ* 30: 43-54.
23. Chuvieco E, Riano D, Aguado I, Cocero D (2002) Estimation of fuel moisture content from multitemporal analysis of Landsat Thematic Mapper reflectance data: application in fire danger assessment. *Int J Remote Sens* 23: 2145-2162.
24. Dennison PE, Roberts DA, Peterson SH, Rachel J (2005) Use of normalized difference water index for monitoring live fuel moisture. *Int J Remote Sens* 26: 1035-1042.
25. Goodwin NR, Coops NC, Wulder MA, Gillanders S, Schroeder TA, et al. (2008) Estimation of insect dynamics using a temporal sequence of Landsat data. *Remote Sens Environ* 112: 3680-3689.
26. Potter CS (2015) Assessment of the immediate impacts of the 2013-2014 drought on ecosystems of the California central coast. *West N Am Naturalist* 75: 129-145.
27. Van Gunst KJV, Weisberg P J, Yang J, Fan Y (2015) Do denser forests have greater risk of tree mortality: A remote sensing analysis of density-dependent forest mortality. *Forest Ecol Manag* 359: 19-32.
28. Hanak E, Mount J, Chappelle C (2014) California's Latest Drought, Public Policy, Institute of California, February 2014.
29. Belmecheri S, Babst F, Wahl E, Stahle D, Trouet V (2015) Multi-century evaluation of Sierra Nevada snowpack. *Nature Clim Change* 6: 2-3.
30. Miller JD, Safford H (2012) Trends in wildfire severity: 1984 to 2010 in the Sierra Nevada, Modoc Plateau, and southern Cascades, California, USA. *Fire Ecol* 8: 41-57.
31. Safford HD, Van de Water K, Schmidt D (2011) California Fire Return Interval Departure (FRID) map, 2010 version. USDA Forest Service, Pacific Southwest Region and The Nature Conservancy-California.
32. Rundel P, Kaufman J, Nathan S, Weixelman D (2007) Montane and subalpine vegetation of the Sierra Nevada and Cascade Ranges. In: Barbour, MG Major (3rd edn.). *J Terrestrial vegetation of California*. New York, USA, pp: 559-599.
33. Lutz JA, Wagtenonk JW, Franklin JF (2009) Twentieth-century decline of large diameter trees in Yosemite National Park, California, USA. *Forest Ecol Manag* 257: 2296-2307.
34. Trujillo E, Molotch NP, Goulden ML, Kelly AE, Bales RC (2012) Elevation-dependent influence of snow accumulation on forest greening. *Nat Geosci* 5: 705-709.
35. Chander G, Markham B, Helder D (2009) Summary of current radiometric calibration coefficients for Landsat MSS, TM, ETM+, and EO-1 ALI sensors. *Remote Sens Environ* 113: 893-903.
36. Masek JG, Vermote EF, Saleous N, Wolfe R, Hall FG, et al. (2006) A Landsat surface reflectance data set for North America, 1990-2000. *GRL* 3: 68-72.
37. Miller JD, Yool SR (2002) Mapping forest post-fire canopy consumption in several overstory types using multi-temporal Landsat TM and ETM data. *Remote Sens Environ* 82: 481-496.
38. Lozano FJ, Suárez-Seoane S, De Luis E (2007) Assessment of several spectral indices derived from multi-temporal Landsat data for fire occurrence probability modeling. *Remote Sens Environ* 107: 533-544.
39. Gelman A, Hill J (2007) Data analysis using regression and multilevel/hierarchical models. Cambridge University Press, New York, New York, USA.
40. Kapnick S, Hall A (2010) Observed climate-snowpack relationships in California and their implications for the future. *J Clim* 23: 3446-3456.
41. Dolanc CR, Thorne JH, Safford HD (2013) Widespread shifts in the demographic structure of subalpine forests in the Sierra Nevada, California, 1934 to 2007. *Global Ecol Biogeogr* 22: 264-276.
42. McIntyre PJ, Thorne JH, Dolanc CR, Flint AL, Flint LE, et al. (2015) Twentieth-century shifts in forest structure in California: Denser forests, smaller trees, and increased dominance of oaks. *Proceedings of the National Academy of Sciences* 112: 1458-1463.
43. Kashian DM, Turner MG, Romme WH (2005) Variability in leaf area and stemwood increment along a 300-year lodgepole pine chronosequence. *Ecosystems* 8: 48-61.
44. Knight DH, Fahey TJ, Running SW (1985) Water and nutrient outflow from contrasting lodgepole pine forests in Wyoming. *Ecol Model* 55: 29-48.
45. Peterson DL, Arbaugh MJ, Lardner MA (1989) Leaf area of lodgepole pine and whitebark pine in a subalpine Sierra Nevada forest. *Can J For Res* 19: 401-403.
46. Ceccato P, Flasse S, Gregoire, J. (2002) Designing a spectral index to estimate vegetation water content from remote sensing data: Part 2. Validation and applications. *Remote Sens Environ* 82: 198-207.
47. Smith TF, Rizzo DM, North M (2005) Patterns of mortality in an old-growth mixed- conifer forest of the southern Sierra Nevada, California. *Forest Science* 51: 266-275.
48. Allen CD, Macalady AK, Chenchouni H, Bachelet D, McDowell N, et al. (2010) A global overview of drought and heat-induced tree mortality reveals emerging climate change risk for forests. *Forest Ecol Manag* 259: 660-684.
49. Guarin A, Taylor AH (2005) Drought triggered tree mortality in mixed conifer forests in Yosemite National Park, California, USA. *Forest Ecol Manag* 218: 229- 244.
50. Asner GP, Nepstad D, Cardinot G, Ray D (2004) Drought stress and carbon uptake in an Amazon forest measured with spaceborne imaging spectroscopy. *Proc Natl Acad Sci USA* 101: 6039-6044.
51. Nepstad DC, Moutinho P, Dias MB, Davidson E, Cardinot G, et al. (2002) The effects of partial throughfall exclusion on canopy processes, aboveground production, and biogeochemistry of an Amazon forest. *J Geophys Res* 107: 1-18.

52. Asner GP, Alencar A (2010) Drought impacts on the Amazon forest: the remote sensing perspective. *New Phytologist* 187: 569-578.
53. Pu R, Kelly M, Anderson GL, Gong P (2008) Using CASI hyperspectral imagery to detect mortality and vegetation stress associated with a new hardwood forest disease. *Photogramm Eng Remote Sens* 74: 65-75.